

# Performance of the reconstruction, calibration and identification of electrons and photons with the ATLAS detector

---

**Sarah Heim**<sup>\*†</sup>

*University of Pennsylvania (US), now at DESY (DE)*

*E-mail: [sarah.heim@cern.ch](mailto:sarah.heim@cern.ch)*

The performance of the reconstruction, calibration and identification of electrons and photons with the ATLAS detector at the LHC is a key component to realize the ATLAS full physics potential, both in the searches for new physics and in precision measurements. Updates to the algorithms used for the reconstruction and identification of electrons and photons with the ATLAS detector during LHC run 2 are presented. Measurements of the identification efficiencies are derived from data. The results from the 2015 and partial 2016  $pp$  collision data set at  $\sqrt{s} = 13$  TeV are reported. Improvements to the electron and photon energy calibration procedure and its performance are also discussed.

*38th International Conference on High Energy Physics*

*3-10 August 2016*

*Chicago, USA*

---

<sup>\*</sup>Speaker.

<sup>†</sup>On behalf of the ATLAS Collaboration.

## 1. Introduction

Electrons and photons are excellent probes in the search for interesting signatures in LHC  $pp$  collisions. They are important for all aspects of the ATLAS [1] physics program, for example precision electroweak measurements, the Higgs discovery and Higgs property studies, as well as new physics searches, like the high mass  $\gamma\gamma$  search [2, 3]. It is crucial for all analyses that use electrons and photons, that the reconstruction efficiencies are high, the background is rejected well, and the energies are measured precisely. In addition, a very good understanding of the systematic uncertainties is crucial.

The focus of this note is to summarize the changes and improvements in electron and photon reconstruction, calibration and identification for the LHC run 2 (which started in 2015) and in particular for 2016. More details, especially on the algorithms and methods themselves, can be found in Refs. [4–9]. A big challenge for LHC run 2 is the increase in the number of interactions per bunch crossing (pile-up), as overlapping events degrade the distinguishing features of electrons and photons. The maximum number of interactions was  $\sim 50$  at the time of ICHEP 2016, compared to  $\sim 25$  in run 1. Another challenge are the gas leaks in the Transition Radiation Tracker (TRT). Because the leaking gas contains a large fraction of Xenon, parts of the TRT had to be filled with Argon, which is cheaper, but does not capture transition radiation as well as Xenon, leading to a decrease in differentiating power between relativistic electrons and hadronic jets.

## 2. Reconstruction

Electrons are reconstructed from an energy cluster in the electromagnetic calorimeter and a matching track in the inner tracking detectors. Special care is taken to account for Bremsstrahlung in the track pattern recognition, as well as the track fit, by allowing to take into account energy loss at every surface point in the detector.

Photons are reconstructed from an energy cluster in the electromagnetic calorimeter, and, in the case of photon-to-electron-pair conversions, matching tracks. Both double and single track conversions are included, to increase the reconstruction efficiency. In the case of single-track conversions, it is assumed that one of the tracks is not reconstructed, p.ex. due to very low energy. The classification into electrons, unconverted and converted photons is based on the compatibility of the tracks to originate from a secondary vertex.

## 3. Identification

Not every object reconstructed as an electron (photon) is a prompt electron (photon) from the collision vertex. Electrons can be faked by hadronic jets, or be the result of heavy flavor decays and converted photons. The situation is similar for photons, which can be faked by hadronic jets, electrons or be part of hadronic jets that include photons. Identification selections drastically reduce the background efficiencies. The identification selections are based on the properties of the reconstructed objects, such as tracks measured in the inner tracking detectors, showers in the electromagnetic and the hadronic calorimeters, as well as track–cluster matching qualities. Isolation requirements are often applied to the identified electrons and photons, helping to reduce the background efficiencies even more.

For the LHC run 2, the identification selections were improved to cope with the high pile-up expectations, as well as changes to the detector: A new innermost tracking layer, the IBL, was inserted during the shut-down between run 1 and run 2. Furthermore, a new variable, the TRT high threshold probability, was introduced to compensate for losses in discrimination power due to the replacement of Xenon with Argon in parts of the TRT.

The standard electron identification on ATLAS is based on a multivariate analysis (MVA). A likelihood (LH) discriminator is formed from most of the discriminating variables (the number of hits in the tracking detectors are required as selection cuts on top of the LH). The discriminator decision depends on the transverse momentum  $E_T$  and the pseudo-rapidity  $|\eta|$  of the electron candidate, as well as the pile-up in the event. Three operating points with decreasing signal and background efficiencies were chosen: LooseLH, MediumLH, and TightLH. For run 2, the LH identification is also used in the trigger selection (in run 1, the trigger selection was cut-based only). Furthermore, the efficiencies versus the transverse momentum were smoothed to allow for a parametrization of both efficiencies and uncertainties. This is important for precision measurements, like the  $W$ -mass measurement. In order to help searches for high mass resonances, the efficiencies at high transverse momenta ( $>300$  GeV) were increased.

The photon identification on ATLAS is based on independent selection cuts on the discriminating variables. The selection cuts depend on the  $|\eta|$  of the photon candidate. They are tuned separately for converted and unconverted photons. Two operating points with decreasing signal and background efficiencies were chosen: Loose and Tight.

#### 4. Efficiency measurements

Efficiencies of the identification of electrons and photons are measured in data. The challenge is to create a pure, unbiased sample on which to probe the efficiencies. Efficiency correction factors are formed from the ratio of efficiencies measured in data and in the Monte Carlo (MC) simulation, and applied to the simulated samples. This correction to the simulation is needed due to known mismodellings of the electromagnetic shower shapes and TRT high threshold probabilities in the ATLAS detector simulation [10–12]. Electron reconstruction and isolation efficiency measurements are discussed in Ref. [5]. The data efficiencies are found to agree well with the simulation.

For electrons, the tag-and-probe method is applied to events consistent with  $Z \rightarrow ee$  and  $J/\psi \rightarrow ee$  decays, requiring the tag to pass strict identification cuts. Remaining backgrounds are subtracted using the invariant mass distributions as discriminating variable. For  $Z \rightarrow ee$ , the isolation distribution of the probe is also used. Figure 1 shows the results of the electron identification measurement based on a subset of the 2016 data and the corresponding simulated  $Z \rightarrow ee$  sample. In addition to the mismodelling discussed above, the simulated sample was produced assuming a TRT gas configuration with more modules filled with Xenon than was possible for the recorded data. The precision of the efficiency measurements for run 1 and 2015 data for electrons with  $35 \text{ GeV} < E_T < 40 \text{ GeV}$  is 0.2%. The preliminary estimates for 2016 are extrapolated from 2015 and therefore have larger uncertainties.

In order to estimate the background contamination in the photon probe samples, several methods are used. The tag-and-probe method is applied to  $Z \rightarrow \ell\ell\gamma$  (with  $\ell = e, \mu$ ) events, estimating

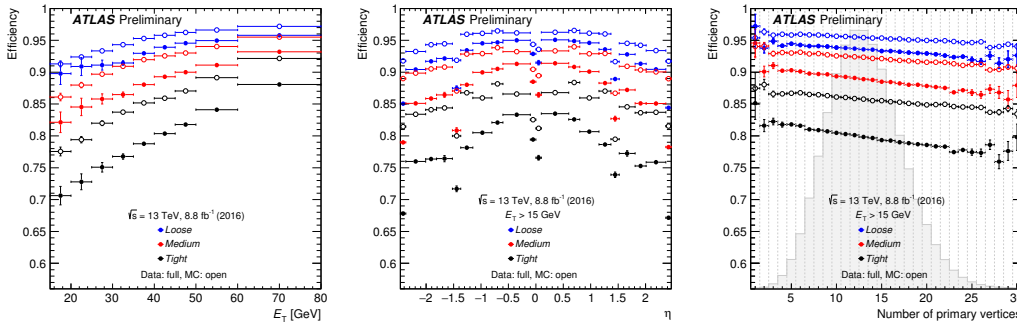


**Figure 1:** Electron identification efficiencies of  $Z \rightarrow ee$  events, measured for a subset of 2016 data and in the simulation [13]. Efficiencies are shown as a function of  $E_T$  (left),  $\eta$  (center), and pile-up (right). On the right, the pile-up distribution of the corresponding data set is overlaid.

the background based on the invariant mass distribution and testing the selection criteria on the photon probe. Other methods are the matrix method based on the isolation distribution of the photon and the background objects, as well as a method that measures the efficiency of the photon identification selection using probe electron showers from a  $Z \rightarrow ee$  tag-and-probe sample, after correcting the electron shower shape variables by the expected difference between photon and electron shower shapes. The three methods cover different ranges in  $E_T$ . It has been shown that they agree well in the overlapping ranges. For photons, first a correction is applied to the shape of the variables in the simulation, which is based on comparing shapes in data and MC. The data-MC correction factors are calculated as a next step and based on the variable-corrected simulation. Figure 2 shows the photon identification efficiencies measured using  $Z \rightarrow \ell\ell\gamma$  events in a subset of the 2016 data, as a function of  $E_T$ . The discriminating variables are already corrected in the simulated sample. The precision of the efficiency measurements for run 1 and 2015 data for photons with

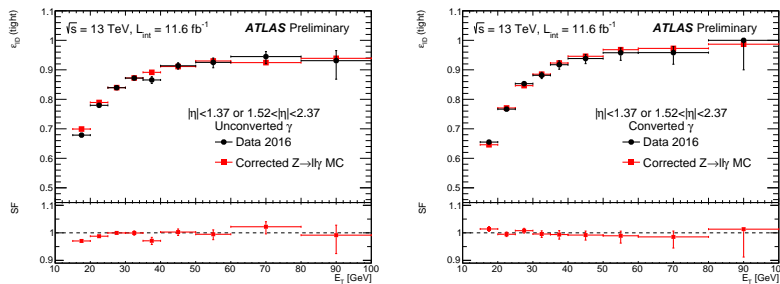


**Figure 2:** Photon identification efficiencies measured with  $Z \rightarrow \ell\ell\gamma$  events in a subset of the 2016 data and in a simulated  $Z \rightarrow \ell\ell\gamma$  sample, for unconverted (left) and converted (right) photons [14]. The discriminating variables are already corrected in the simulated sample based on data-MC comparisons. The resulting correction factors are shown in the bottom panel.

$35 \text{ GeV} < E_T < 40 \text{ GeV}$  is 1–2%. The preliminary estimates for 2016 are extrapolated from 2015 and therefore have larger uncertainties.

## 5. Calibration

The calibration of electrons and photons is performed in multiple steps. First an electronic-readout calibration is applied, followed by precorrections, accounting for effects due to the bunch-train structure and additional response variations. An MVA is trained on a simulated single-electron (photon) MC sample, using as input the energy measurements in the different calorimeter layers, as well as the position of the electron (photon) cluster, and, for photons, conversion information. The resulting electron energies are used to make a comparison of the  $Z \rightarrow ee$  mass peak shape between data and simulation, adjusting the energy scale in data to match the one in simulation, and the resolution in the simulation to match the data. The determined scales and resolution parameters are propagated to photons.

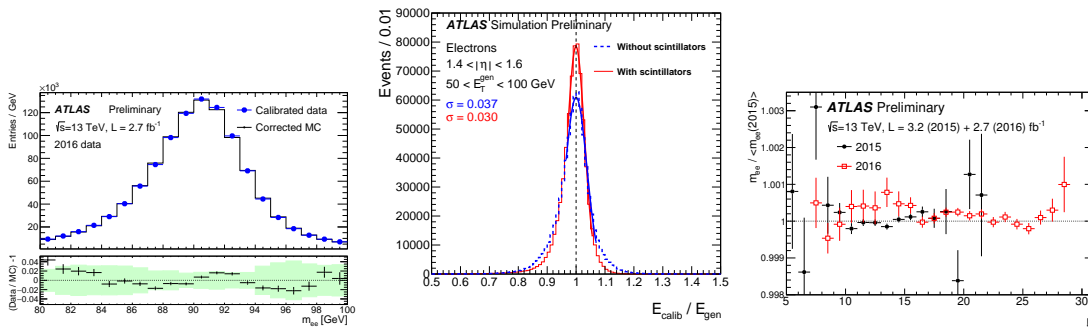


**Figure 3:** Left: Invariant mass of dielectron events, comparing a subset of the calibrated 2016 data to the corrected simulation. Center: Improvement of the electron energy reconstruction in the calorimeter gap due to the inclusion of the energy measured in the tile scintillators in the energy calibration procedure. Right: Stability of the electron energy scale, represented by the ratio of reconstructed invariant dielectron mass to the average mass, as a function of pile-up for 2015 and 2016 data, represented by the average interactions per bunch-crossing  $\mu$ . All three plots can be found in Ref. [9].

The run 2 calibration was updated wrt. run 1 to take into account the IBL. Furthermore, the calibration was extended to also cover the transition region between the barrel and endcap of the electromagnetic calorimeter,  $1.4 < |\eta| < 1.6$ , which suffers from large amounts of material that degrades the energy resolution of traversing particles. To cope with the material, the energy measurements of the scintillators of the tile calorimeter that are situated in the transition region are included in the MVA. Figure 3, center, shows the resulting improvement of the electron energy reconstruction in the calorimeter transition region. The improvements for converted and unconverted photons are very similar. The invariant mass of dielectron events, comparing calibrated 2016 data to corrected simulation, is shown in Fig. 3, left. It can be seen that the peak shape is described by the simulation within the uncertainties. Figure 3, right, shows that the energy scale remains stable as a function of pile-up. The full evaluation of the calibration uncertainties with run 2 data is currently ongoing.

## 6. Summary

Challenges and improvements of electron and photon reconstruction, calibration and identification were presented. They include the larger pile-up, changes to the detector, and improvements

of the methodologies. The performance of the electron and photon algorithms for a subset of 2016 data was presented. The reached precisions are close to run 1 for the efficiency measurements already, while the full evaluation of uncertainties for the calibration is still ongoing.

## References

- [1] ATLAS Collaboration, *The ATLAS Experiment at the CERN Large Hadron Collider*, *JINST* **3** (2008) S08003.
- [2] ATLAS Collaboration, *Search for resonances in diphoton events at  $\sqrt{s}=13$  TeV with the ATLAS detector*, *JHEP* **09** (2016) 001, [[1606.03833](#)].
- [3] ATLAS Collaboration, *Search for scalar diphoton resonances with  $15.4 \text{ fb}^{-1}$  of data collected at  $\sqrt{s}=13$  TeV in 2015 and 2016 with the ATLAS detector*, *ATLAS-CONF-2016-059* (<https://cds.cern.ch/record/2206154>), 2016.
- [4] ATLAS Collaboration, *Electron efficiency measurements with the ATLAS detector using the 2012 LHC proton-proton collision data*, *ATLAS-CONF-2014-032* (<http://cds.cern.ch/record/1706245>), 2014.
- [5] ATLAS Collaboration, *Electron efficiency measurements with the ATLAS detector using the 2015 LHC proton-proton collision data*, *ATLAS-CONF-2016-024* (<http://cds.cern.ch/record/2157687>), 2016.
- [6] ATLAS Collaboration, *Measurement of the photon identification efficiencies with the ATLAS detector using LHC Run-1 data*, [1606.01813](#).
- [7] ATLAS Collaboration, *Photon identification in 2015 ATLAS data*, *ATL-PHYS-PUB-2016-014* (<http://cds.cern.ch/record/2203125>), 2016.
- [8] ATLAS Collaboration, *Electron and photon energy calibration with the ATLAS detector using LHC Run 1 data*, *Eur. Phys. J.* **C74** (2014) 3071, [[1407.5063](#)].
- [9] ATLAS Collaboration, *Electron and photon energy calibration with the ATLAS detector using data collected in 2015 at  $\sqrt{s} = 13$  TeV*, *ATL-PHYS-PUB-2016-015* (<http://cds.cern.ch/record/2203514>), 2016.
- [10] ATLAS Collaboration, *Electron performance measurements with the ATLAS detector using the 2010 LHC proton-proton collision data*, *Eur. Phys. J.* **C72** (2012) 1909, [[1110.3174](#)].
- [11] GEANT4 collaboration, S. Agostinelli et al., *GEANT4: A Simulation toolkit*, *Nucl. Instrum. Meth.* **A506** (2003) 250–303.
- [12] ATLAS Collaboration, *The ATLAS Simulation Infrastructure*, *Eur. Phys. J.* **C70** (2010) 823–874, [[1005.4568](#)].
- [13] ATLAS Collaboration, *Electron identification efficiency measured with  $Z \rightarrow ee$  events using 2016 data*, *Public Plots* (<https://atlas.web.cern.ch/Atlas/GROUPS/PHYSICS/PLOTS/EGAM-2016-002/index.html>), 2016.
- [14] ATLAS Collaboration, *Photon Identification Efficiencies using 2016 Data with radiative Z boson decays*, *Public Plots* (<http://atlas.web.cern.ch/Atlas/GROUPS/PHYSICS/PLOTS/EGAM-2016-003/index.html>), 2016.